Effects of ZIF-L Morphology on PI@PDA@PEI/ZIF-L Composite Membrane's Adsorption and Separation Properties for Heavy Metal Ions

HUI CAO , Ziyue Jiang , Jing Tang , Qiong Zhou *

Posted Date: 11 October 2023

doi: 10.20944/preprints202310.0653.v1

Keywords: ZIF-L; Nanofibers; Heavy metal separation membrane; Heavy metal ions; Filtration rate; Permeability

Article

Effects of ZIF-L Morphology on PI@PDA@PEI/ZIF-L Composite Membrane's Adsorption and Separation Properties for Heavy Metal Ions

Hui Cao [1], Ziyue Jiang [2], Jing Tang [3] and Qiong Zhou [1,*]

[1] China University of Petroleum, Beijing, China, 102249; candy1128a@163.com
[2] The Experimental High School Attached to Beijing Normal University, Beijing 102249, China; sophia20220129@163.com
[3] China University of Petroleum, Beijing 301617, China; tangjinggfz@163.com
* Correspondence: zhouqiong_cn@163.com

Abstract: Composite polymolecular separation membranes were prepared by combining multi-branched ZIF-L with high porosity electrospinning nanofibers PI. Meanwhile, PDA and PEI were introduced into the membrane in order to improve its adhesion. The new membrane is so called "PI@PDA@PEI/ZIF-L-4" composite membrane; compared with PI@PDA@PEI/ZIF-8 composite membrane, the new membrane's filtration rates for heavy metal ions such as Cd^{2+}, Cr^{3+} and Pb^{2+} were increased by 7.0%, 6.6% and 9.3%, respectively. Furthermore, the new membrane has a permeability up to 1,140.0 $L{\cdot}m^{-2}{\cdot}h^{-1}{\cdot}bar^{-1}$, and were presenting a very stable performances after four repeated uses. The separation mechanism of PI@PDA@PEI/ZIF-L composite membranes was further analyzed in order to provide a base support for producing separation membranes with high barrier rate and high flux.

Keywords: ZIF-L; Nanofibers; Heavy metal separation membrane; Heavy metal ions; Filtration rate; Permeability

1. Introduction

Heavy metal ions due to their low concentration, high solubility, and tendency to form complexes are difficult to be removed/filtered from the polluted water [1]. This becomes a challenging subject and draws some recent interests [2–4]. For the purpose of heavy metal ion separation, metal-organic frameworks (MOFs) have become an important research focus for their high specific surface area and porosity, high active site, adjustable structure, and easy functionalization.

Existing study on adsorbent materials commonly focus on the adsorption capacity of adsorbents for heavy metals in single-component heavy metal solutions; few research articles have published for such in multi-component heavy metal solutions. For real cases of sewage treatments, however, a variety of heavy metals coexist in sewage/the polluted waters. It is extremely important to study the removal of adsorbents in multi-component heavy metal solutions.

Flower-shaped zeolitic imidazolate framework-L (ZIF-L) nanostructures, as a MOF material, has unique cushion cavities that can capture heavy metal ions. The free 2-methylimidazole in the cavity can also provide additional adsorption sites. ZIF-L is expected to have excellent heavy metal ion adsorption capacity. Electrospinning is a convenient and effective method typically to produce functional nanofibrous membranes (NFMs). The prepared NFMs have the advantages of high porosity, large specific surface area, adjustable structure, and easy surface modification.

In the present study, ZIF-L was anchored onto the surface of PI fibers by PEI coating, and the synthesized PI@PDA@PEI/ZIF-L-4 composite membrane was used to separate heavy metal ions in the polluted water. It is desirable to achieve an increase of water flux and heavy metal removal rate under low pressure conditions.

Preprints (www.preprints.org) | NOT PEER-REVIEWED | Posted: 11 October 2023 doi:10.20944/preprints202310.0653.v1

2. Experimental Part

2.1. Materials

Materials, such as Pyromellitic dianhydride (PMDA), 4,4 '-diamino-diphenyl ether melamine (ODA), polyethylenimide (PEI), 2-methylimidazole, zinc nitrate hexahydrate (Zn $(NO_3)_2$•$6H_2O$), hydrogen peroxide (H_2O_2), dopamine (DA), lead acetate, cadmium nitrate, chromium trichloride, and the standard solution of disodium ethylenediamine tetraacetate, were purchased products from Victrex company.

2.2. Preparation of ZIF-L

Based on the coordination control method, flower-shaped zeolitic imidazolate framework-L (ZIF-L) crystals were successfully synthesized at room temperature by adding H_2O_2 as the control agent. 30% H_2O_2 solution (0,1,2,3,4,5 mL) was added to an aqueous solution of 2-methimidazole and slowly stirred for 2 minutes. The obtained ZIF-L were recorded as ZIF-L-0 (ZIF-8), ZIF-L-1, ZIF-L-2, ZIF-L-3, ZIF-L-4 and ZIF-L-5[5]

2.3. Preparation of PI@PDA@PEI/ZIF-L composite Membrane

As shown in Figure 1, PDA@PI fibers were obtained from the following steps:

(1) Use 0.02422g of THP (Tetrahydropyran) dissolved in 50ml of deionized water to conFigure 4 mmol/L of the THP solution;
(2) Take 0.1g HCl (Hydrochloric acid) with appropriate amount of deionized water to make 30 ml HCl solution;
(3) Drop 1.5g HCl solution (from step2) into THP solution (from step1) to obtain a mixed solution of PH 8.5;
(4) Add 0.2g of dopamine (DA) to the above mixed solution (from step3) and settle it to 100ml, and 2 mg/ml of the PDA solution was obtained;
(5) Put two PI nanofibers of 5x5cm into the PDA solution (mixed in step4), and then removed them out after 24 hours to obtain PDA@PI fibers with PDA coated on the surface.

Figure 1. Schematic diagram of preparation of PI@PDA@PEI/ZIF-L composite membrane.

To obtain the PI@PDA@PEI/ZIF-L composite membrane, by adding 5 wt.% ZIF-L-4 into 3 wt.% PEI solution, then stirring and applying the above solution to the PDA@PI fiber surfaces, until the liquid completely covers the entire surfaces of the fibers. After drying the fiber film in an oven at 80 °C, a PI@PDA @PEI/ZIF-L membrane was obtained

2.4. Characterization

The sample morphology was characterized by scanning electron microscope (SEM, SU8010). The SEM characterization and associated element analysis were performed by Hitachi SU8010 equipped with energy dispersion X spectroscopy (EDS). Fourier transform infrared spectroscopy (FTIR, Tensor Ⅱ) can characterize the types of functional groups and the interactions between the functional groups in a sample. The attenuated total reflection method (ATR) is used for testing of membranes, with a scanning range from 4000 cm^{-1} to 650 cm^{-1}, and the transmission method (TR) is used for testing of

Preprints (www.preprints.org) | NOT PEER-REVIEWED | Posted: 11 October 2023 doi:10.20944/preprints202310.0653.v1

powdered samples, with a scan range from 4000cm^{-1} to 400cm^{-1}. The crystal structure was determined by performing X-ray diffraction (XRD, D8 Focus) on the sample. The test conditions were using the Cu Kα target with a wavelength of 0.154 nm, the test angle of 5~70°, the voltage of 40 kV, the current of 30 mA, and the scan rate of 5°/min. The composition and structure of the sample can be tested by X-ray photoelectron spectroscopy.

2.5. Performance Characteristics

Heavy metal adsorption performance test

A solution containing three-component heavy metals, e.g., Pb^{2+}, Cd^{2+}, and Cr^{3+} was prepared, and the PH of the solution was adjusted to 6 by adding dilute hydrochloric acid. The solution in 20ml was added with a certain amount of ZIF-L, and stirred at room temperature for 10 minutes. After the adsorption process is completed, the needle filter is used to filter the solution. The concentration of the filtered solution is measured by an inductively coupled plasma spectrometer (ICP), and the adsorption capacity and adsorption rate are calculated by the following formula:

$$R = \left(1 - \frac{C}{C_0}\right) \times 100\% \quad (1)$$

$$q = \frac{V(C_0 - C)}{m} \quad (2)$$

Where, C_o is the initial mass concentration, mg/L; C is the mass concentration at the adsorption equilibrium (C_e) or time t (min), mg/L; V is the volume of solution, L; m is the mass of the adsorbent, g.

Membrane water flux test

The permeability and barrier properties of the membranes were evaluated by a self-made device for cross-flow filtration (Figure 2). This filter device is composed of two polytetrafluoroethylene plates engraved with serpentine water channels, with an effective filtration area of 6.326×10^{-4}m^2. Filtration power is provided by two peristaltic pumps.

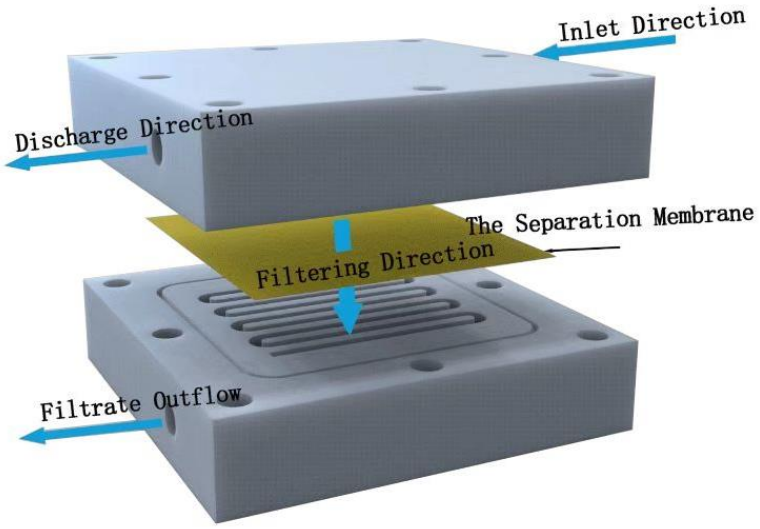

Figure 2. Schematic diagram of self-made experimental device for cross-flow filtration.

Place the separation membrane (to be tested) into the cross-flow filter device, ensure that the membrane completely covers the flow path, and then secure it with screws. Firstly, the deionized water is pre-compressed for 10 minutes at 2 bar pressure to obtain a stable water flux. Time duration was measured for filtering out 20ml deionized water at 1 bar water pressure. Multiple tests were then

Preprints (www.preprints.org) | NOT PEER-REVIEWED | Posted: 11 October 2023 doi:10.20944/preprints202310.0653.v1

repeated, and the average value of the measured times was used to calculate the flow rate of the filtered liquid. The following formula is used to calculate the water flux of the membrane:

$$J=v/(S\times P) \quad (3)$$

Where J ($L\bullet m^{-2}\bullet h^{-1}\bullet MBar$) is the water flux, v ($L\bullet h^{-1}$) is the flow rate of the filtered liquid, S ($6.326\times10^{-4}m^2$) is the effective filtration area, and P (Bar) is the pressure applied on the membrane.

3. Results and Discussion

3.1. Structure Characterization and Adsorption Properties of ZIF-L

Figure 3 shows the SEM images of the ZIF-L series crystals. As shown in Figure 3, with more addition of H_2O_2, the ZIF-L gradually grows into a flower-shaped structure with elongated branches, and such branches on the crystal surface increase in number and become longer and thinner. The observation is consistent with the description in the published literature [6].

The formation mechanism of flower-shaped ZIF-L structures can be understood as a two-step crystal growth process. Zn^{2+} first binds with 2-methyl imidazole to form the ZIF-L core, and then H_2O_2 adsorbed onto the crystal core causes lattice accumulation layer by layer through hydrogen bonding, enabling the lateral and epitaxial growth of the crystal core. With the increase of H_2O_2 concentration, the number of H_2O_2 molecules adsorbed onto the core surface increases, and the growth site also increases. Due to steric hindrance, the core surface tends to epitaxial growth, resulting in an increased number of elongated branches on the crystal surface.

For ZIF-L-5, in the SEM image, some broken branches were found, possibly due to the branches of ZIF-L-5 are too slender and unstable during ultrasound process. However, no broken branches were observed in the morphology analysis of ZIF-L-3 and 4; this indicates that ZIF-L-3 and 4 in ZIF-L structures are more stable.

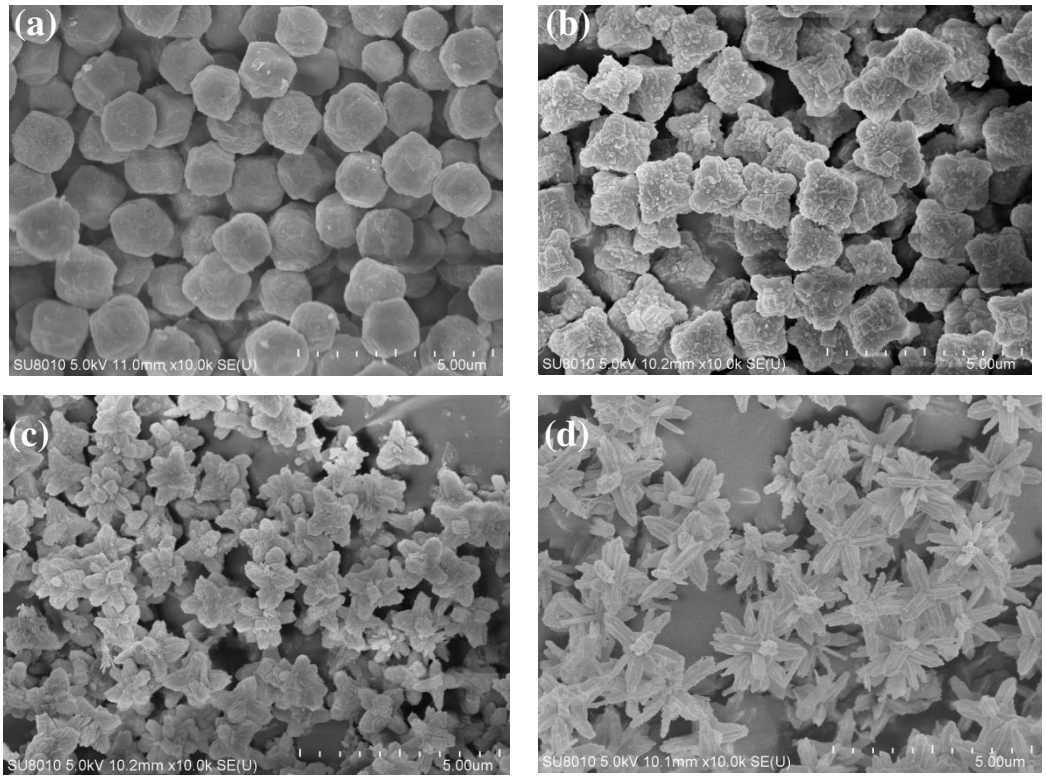

Preprints (www.preprints.org) | NOT PEER-REVIEWED | Posted: 11 October 2023 doi:10.20944/preprints202310.0653.v1

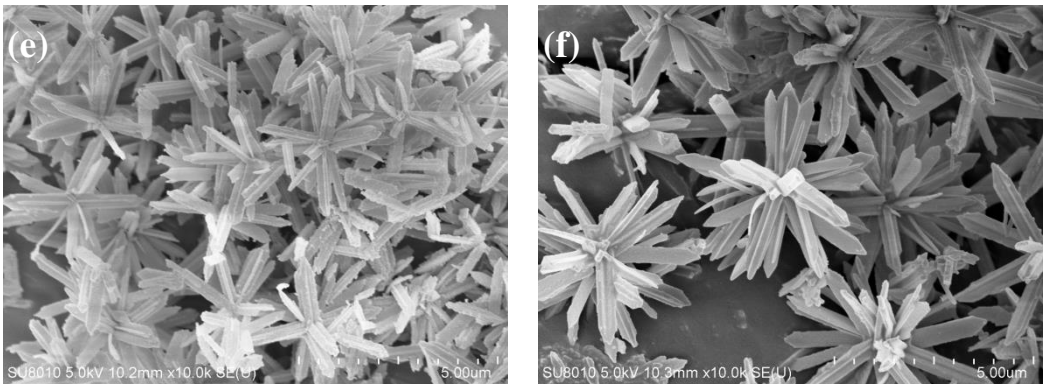

Figure 3. SEM images of ZIF-L crystals obtained when adding. (**a**) 0 mL, (**b**) 1 mL, (**c**) 2 mL, (**d**)3 mL, (**e**)4 mL, and (**f**) 5 mL H_2O_2

In Figure 4a, ZIF-8 and ZIF-L-1, at 011,002,022,013 and 222, demonstrated the successful synthesis of ZIF-8 and ZIF-L[7]. It is also noticed that ZIF-L-1 lacks the characteristic peak of ZIF-L, while ZIF-L-3, 4, and 5 are consistent with the characteristic peak of ZIF-L. This might be due to incomplete crystallization with 1ml H_2O_2, not forming ZIF-L characteristic peak. Adding more H_2O_2, the crystal structure gradually changes to ZIF-L [8], and the ZIF-L-3, 4, and 5 crystals have changed into a stable ZIF-L structure. This demonstrates that the H_2O_2 addition to the ZIF-8 reaction system can transform the ZIF-8 crystal into ZIF-L.

In the FTIR spectrum of Figure 4b, all ZIL-L samples display significant peaks at 756 cm^{-1}, 1146 cm^{-1}, 1307 cm^{-1}, 1422 cm^{-1}, 2920 cm^{-1}, 3134 cm^{-1}, and 3034 cm^{-1}. The peak at 756 cm^{-1} is assigned to out-of-plane bending; peaks at 1146 and 1307 cm^{-1} correspond to in-plane bending; peaks at 1422 and 2920 cm^{-1} correspond to the expansion vibration of the C-H and C= N bonds on the imidazole ring; and peaks at 3134 cm^{-1} correspond to the expansion vibration of the methyl group [9]. Note that a new peak appeared in the last three samples, located at 3034 cm-1, caused by the N-H bond, which was generated as a result of the crystal transition to ZIF-L. Free 2-methylimidazole is dispersed in the middle layer of the ZIF-L phase, so there are many free 2-methylimidazole (a non-crystalline molecule at the amino-binding site) [10].

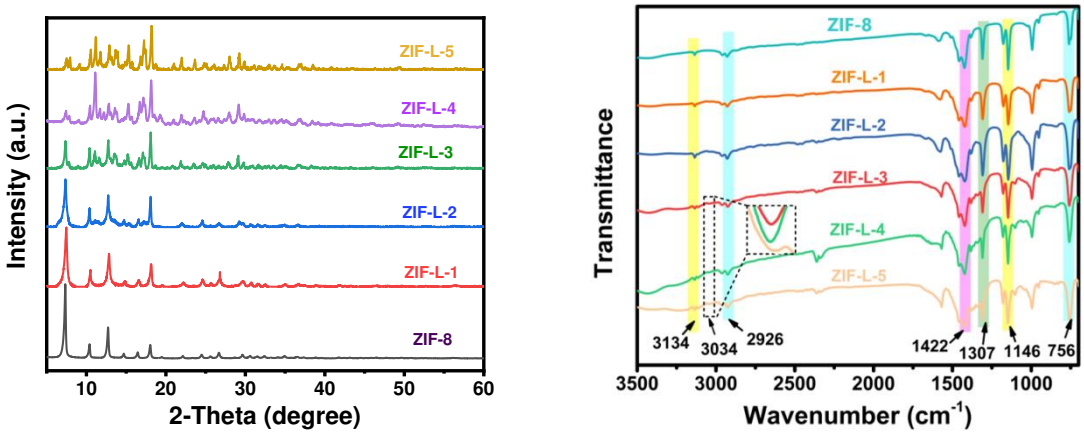

(a) XRD (b) FTIR

Figure 4. The XRD and FTIR characterization plots of ZIF-L.

The adsorption properties of six MOF materials (i.e., ZIF-8, ZIF-L-1, ZIF-L-2, ZIF-L-3, ZIF-L-4 and ZIF-L-5) on heavy metal solutions (including 10 ppm each of Cd^{2+}, Cr^{3+} and Pb^{2+}) are shown in Figure 5.

Preprints (www.preprints.org) | NOT PEER-REVIEWED | Posted: 11 October 2023 doi:10.20944/preprints202310.0653.v1

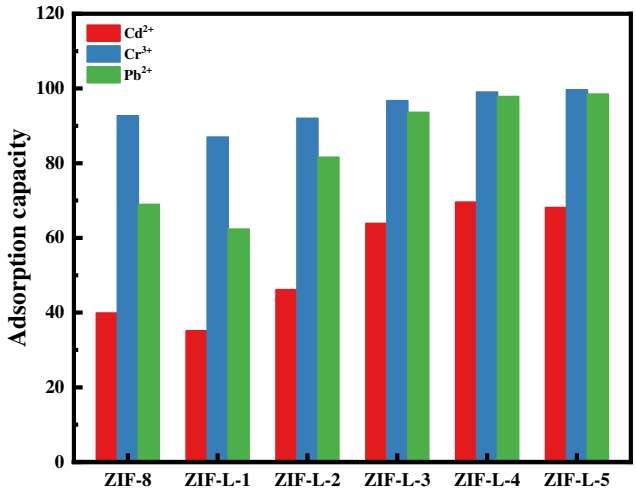

Figure 5. Adsorption of six MOF materials in mixed heavy metal solutions. (including 10 ppm of Cd^{2+}, Cr^{3+}, Pb^{2+}).

It can be seen from Figure 5, the six MOF materials have excellent adsorption capacity for Cd^{2+}, Cr^{3+} and Pb^{2+}. The adsorption abilities are mainly attributed to the ion exchange between ZIF-L and metal cations (cation heavy metals can replace Zn^{2+} site) and coordination (between cations and functional groups-NH-and-OH). In addition, electrostatic attraction also plays a synergistic role in the adsorption process [11].

The principle of adsorption selectivity of ZIF-L series materials to three heavy metals is similar, in an order of Cr^{3+}> Pb^{2+}> Cd^{2+}. This is because the high ions are more likely to be adsorbed; for example, Cr^{3+} is preferentially adsorbed. ZIF-8 has significantly higher selectivity for Cr^{3+}. For Cd^{2+} and Pb^{2+}, with the same valences, the adsorbent usually preferentially adsorbs divalent cations with lower hydration energy; this is because the metal ions must leave most of the hydration water before entering the smaller channel of the adsorbent, and the lower hydration energy is more likely to escape [12]. It was reported that Pb^{2+} hydration energy is 1425 kJ/mol and Cd^{2+} hydration energy is 1755 kJ/mol. Obviously, Pb^{2+} has less hydration energy and is easier to enter the micropores of the adsorbent. The heavy metal ions separated from most of the hydration water are more conducive to interact with the adsorbent functional groups. Therefore, Pb^{2+} prefers Cd^{2+} to be adsorbed [13–15]. This is also consistent with the experimental results of the present study.

The adsorption rates of ZIF-L-1 to ZIF-L-4 in mixed heavy metal solution are gradually increased with higher H_2O_2 addition. Branches from ZIF-L-1 to ZIF-L-4 structures increase in numbers and with elongated lengths, resulting in larger total surface areas in contact with heavy metal ions, thus high mass transfer efficiency. The adsorption capacities of ZIF-L-4 and ZIF-L-5 are barely the same. However, in the SEM images of ZIF-L-5, fragments and broken branches were found, and the branches were too slender and unstable; therefore, ZIF-L-4 was selected as the adsorbent for subsequent studies.

3.2. Characterization of PI@PDA@PEI/ZIF-L-4 Composite Membranes

Electrospinning nanofibers loaded MOFs is a method to produce MOFs into membranes, in which less separation pressure and lower energy consumption are needed compared to the conventional mixed matrix membrane. The commonly used methods to load MOFs on electrospinning nanofibers mainly include co-electrospinning and in situ growth; there are still certain problems such as that active sites of MOFs are buried or easy to fall off from the fiber surface.

Polyethylenimine (PEI) has many forms of amino groups, including primary, secondary, and tertiary functional amine sites. Studies have shown that PEI with coordination and hydrophilicity has excellent adsorption and chelation capacity to heavy metal ions. The present study used PEI as

Preprints (www.preprints.org) | NOT PEER-REVIEWED | Posted: 11 October 2023 doi:10.20944/preprints202310.0653.v1

an adhesive to anchor MOFs to the fibers, and improved the binding force of PEI to PI by grafting polydopamine on PI nanofibers.

To obtain the PI @ PDA @ PEI / ZIF-8 and PI @ PDA @ PEI / ZIF-L nanofiber composite membranes, ZIF-8 and ZIF-L-4 were incorporated into the PEI system and coated onto PDA-modified PI fibers. In which, nanofibers mainly provide support and promote penetration, PEI provides the bonding effect of ZIF onto fibers, and ZIF-L is for the adsorption of heavy metal ions. To explore the effect of ZIF-L morphology on the membrane separation performance, the mechanism of membrane separation was speculated by XPS and EDS.

As shown in Figure 6a,b, the PI nanofibers have a smooth surface and a three-dimensional mesh nanostructure, and the diameter of the filament ranges from 100 to 200 nm. A handful of PDA particles were adhered to the surface of the PI fibers, resulting in increase of the PI fiber diameters to 150~280 nm, along with a corresponding increase in the roughness of the nanofibers.

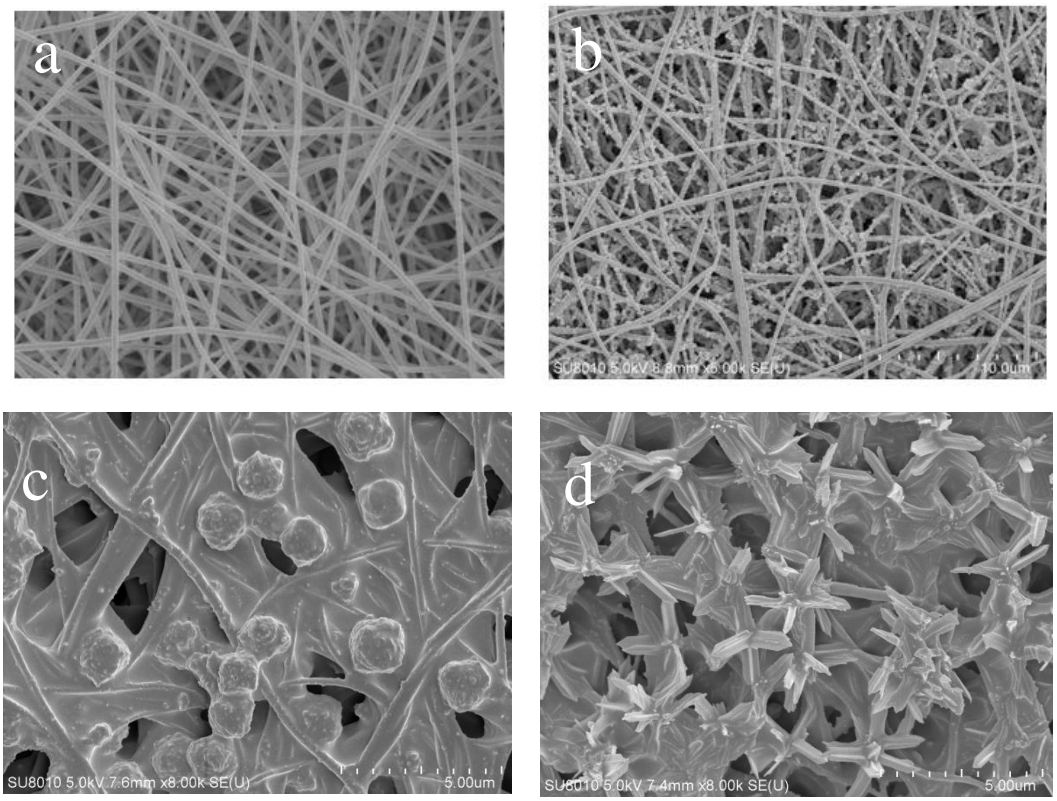

Figure 6. SEM images of different membranes (**a**) PI nano-fiber, (**b**) PI@PDA membrane, (**c**) PI@PDA@PEI /ZIF-8 membrane, (**d**) PI@PDA@PEI /ZIF-L-4 membrane.

From Figure 6c,d, it can be seen that spherical particles of about 2 μm in diameter can be observed on the surface of the composite membrane mixed with ZIF-8, consistent with the morphology of ZIF-8 crystals. The composite membrane incorporated with ZIF-L-4 (PI@PDA@PEI/ZIF-L-4 membrane) was bonded to a large number of flower-shaped ZIF-L-4 crystals with a diameter of approximately 4 μm. The incorporation of PEI binds ZIF-8 and ZIF-L-4 to the fiber through the cross-linking network, binding ZIF-L-4 tightly to the fiber matrix and not easy to fall off.

The composition and structure of the different materials were verified by FTIR and XRD, as shown in Figure 7.

Preprints (www.preprints.org) | NOT PEER-REVIEWED | Posted: 11 October 2023 doi:10.20944/preprints202310.0653.v1

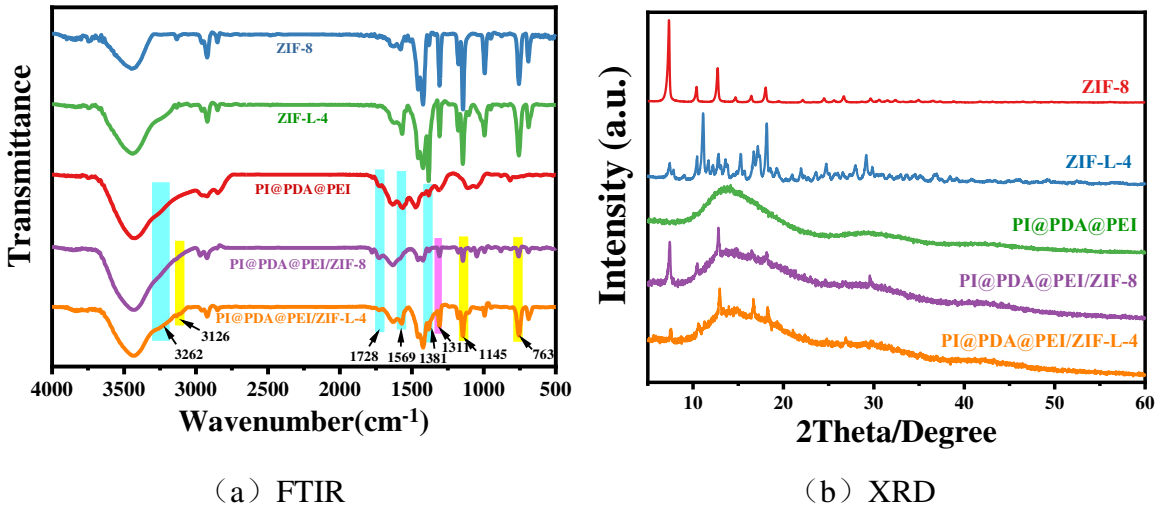

（a）FTIR （b）XRD

Figure 7. FTIR spectra and (**b**) the XRD curve of each component.

As shown from Figure 7a, in the PI@PDA@PEI membrane, distinct characteristic peaks can be observed at 3262 cm^{-1},1569 cm^{-1},1483cm^{-1} and 1580 cm^{-1}. The peaks at 3262 cm^{-1} and 1569 cm^{-1} belong to the bending vibrations of the-NH_2 and-NH in the PEI chain, respectively. The more intense peaks at 1483 cm^{-1} and 1580 cm^{-1} peaks represent the characteristic absorption peaks of the secondary amine and primary amine groups [16,17].

For ZIF-8 and ZIF-L-4, the peak at 756cm^{-1} is assigned to out-of-plane bending; peaks at 1146 and 1307cm^{-1} correspond to in-plane bending; peaks at 1422 and 2926cm^{-1} correspond to the expansion vibration of the C-H and C= N bonds on the imidazole ring; and the peak at 3134 cm^{-1} corresponds to the expansion vibration of the methyl group. Note that a new peak appeared in the last three samples, located at 3034 cm^{-1}, which is caused by the N-H bond. The formation of this bond is the result of the crystal transition to ZIF-L, where the free 2-methimidazole is dispersed in the middle layer of the ZIF-L phase, so there are many free 2-methimidazole (a non-crystalline molecule in the amino binding site) [6].

Compared with PI@PDA@PEI, some new peaks appeared in the PI@PDA@PEI/ZIF-8 and PI@PDA@PEI/ZIF-L-4 composite membranes. The new peak at 3136 cm^{-1} corresponds to the stretching vibration of the methyl group in ZIF-8 and ZIF-L-4, the new peak at 759cm^{-1} corresponds to out-of-plane bending of ZIF-8 and ZIF-L-4, and the new peaks at 1147 and 1308cm^{-1} correspond to in-plane bending of ZIF-8 and ZIF-L-4, demonstrating the successful loading of ZIF-8 and ZIF-L-4.

From the XRD profile of Figure 7b, the diffraction peak of ZIF-8 is consistent with those reported in previous work, where 2 θ are characteristic peaks of 7.3,10.3,12.7,12.7,14.7,16.4 and 18.0 corresponding to (011), (002), (112), (022), (013) and (222) surface [18], demonstrating the successful preparation of ZIF-8. The diffraction peak of ZIF-L-4 agrees with that of ZIF-L as shown in the literature, indicating the successful preparation of ZIF-L-4. The peaks of both composite membranes correspond to the amorphous peaks of the polymer and the major crystallization peaks of ZIF-L. ZIF-L doping is effective, and the topology of all species is preserved after recombination.

To further verify the structure of the composite membrane surface, an XPS analysis was performed on the PI @ PDA @ PEI / ZIF-L-4 composite membrane, as shown in Figure 8. The prepared composite membrane samples showed several characteristic peaks at binding energies of approximately 285.08, 397.08 and 531.8 eV, mainly corresponding to C 1s, N 1s, O 1s and Zn 2 p. In the C1s spectrum, three main peaks can be observed at 287.7, 285.8 and 284.5 eV for C=O, C=N and C=C groups. Among them, the C=O group proves the existence of the PI fiber layer in the composite membrane, the C=N group is the crosslinking reaction between PEI and ECH, and the C=C group proves the presence of 2-methimidazole in PI and ZIF-L.

Preprints (www.preprints.org) | NOT PEER-REVIEWED | Posted: 11 October 2023 doi:10.20944/preprints202310.0653.v1

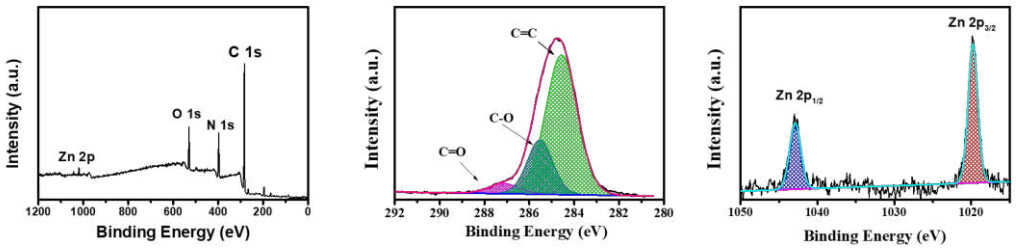

Figure 8. XPS spectra of PI@PDA@PEI/ZIF-L-4 composite films (**a**) Total spectra (**b**) C 1s spectra (**c**) Zn 2p spectra.

High-resolution N 1s spectra (Figure 8) were fitted to two characteristic nitrogen species at 399.2 and 397.4 eV, corresponding to neutral amine (–NH_2/–NH) and protonated amine (–NH_3^+ or -NH_2^+), confirming the binding of PEI in the composite membrane. In addition, two characteristic peaks of Zn were displayed at 1020.6 eV (Zn2p3) and 1043.9 eV (Zn2p1). The above results showed that the PEI / ECH crosslinking system was successfully synthesized on the PI nanofibers and the ZIF-L-4 nanoparticles were successfully loaded on the membrane surface.

3.3. Separation Properties of the PI@PDA@PEI/ZIF-L-4 Composite Membranes

The separation properties of the membrane were determined by permeability experiments. Through the operation of the self-made cross-flow filtration device, the water flux of the membrane was calculated by formula (1), and the heavy metal barrier rate was calculated by measuring the concentration change of heavy metal ions before and after cross-flow filtration by ICP-OES. The operating pressure of the device is 1bar, the test temperature is 25℃, the three-component heavy metal solution is used as the feeding liquid (including Cd^{2+}、Cr^{3+} 、Pb^{2+} each 1ppm), and the solution flow rate is 250 ml/min..

The water flux of PI @ PDA @ PEI / ZIF-8 composite membrane and PI @ PDA @ PEI / ZIF-L-4 composite membrane and the separation performance for heavy metal solutions are shown in Figure 9.

In this experiment, effects of MOF morphology on the separation performances were investigated by doping the membrane with ZIF-8 and ZIF-L-4 in different appearances. As shown in the Figure 9, the flower-shaped ZIF-L-4 can be more assisting to the deposition of PEI on the fiber membrane with more mosaic branching structures, and the crystal branches interlace each other, providing a long-range channel for the transport of water molecules. Therefore, the water molecules stay in the membrane for longer, and the water flux (1140 $L{\cdot}m^{-2}{\cdot}h^{-1}{\cdot}bar^{-1}$) is lower than the water flux of the ZIF-8 composite membrane (1243.44 $L{\cdot}m^{-2}{\cdot}h^{-1}{\cdot}bar^{-1}$).

As seen in Figure 9, the water flux of the PI @ PDA @ PEI / ZIF-L-4 composite membrane is 1140 $L{\cdot}m^{-2}{\cdot}h^{-1}{\cdot}bar^{-1}$, which is lower than such of the ZIF-8 composite membrane (i.e., 1243.44 $L{\cdot}m^{-2}{\cdot}h^{-1}{\cdot}bar^{-1}$). The fact is that, comparing with ZIF-8, the flower-shaped ZIF-L-4 (containing more mosaic branching structures and with branches between crystals cross each other) provides a long-range channel for the transport of water molecules; thus, the water molecules stay in the membrane for longer.

It can also be seen in Figure 9 that by introduction of ZIF-L-4 into the composite membrane, the removal rate of heavy metals was significantly increased. The barrier rate of Cr^{3+} and Pb^{2+} both exceed 90%. The removal rate of Cd^{2+} increased by 7%, from 73.3% to 80.4%; the removal rate of Cr^{3+} increased by 6.6%, from 90.2% to 96.8%; the removal rate of Pb^{2+} increased by 9.3%, from 90.3% to 99.6%. Due to the flower-shaped branching structure of ZIF-L-4, the total surface area of contact with heavy metals is larger than that of ZIF-8. The long-range orderly channels formed by staggered branches enforce great resistance to transmission of heavy metal ions, and also greatly improves the efficiency of heavy metal ions contacting the active site on ZIF-L-4. The adsorption effect of heavy metal ions is much better improved.

Preprints (www.preprints.org) | NOT PEER-REVIEWED | Posted: 11 October 2023 doi:10.20944/preprints202310.0653.v1

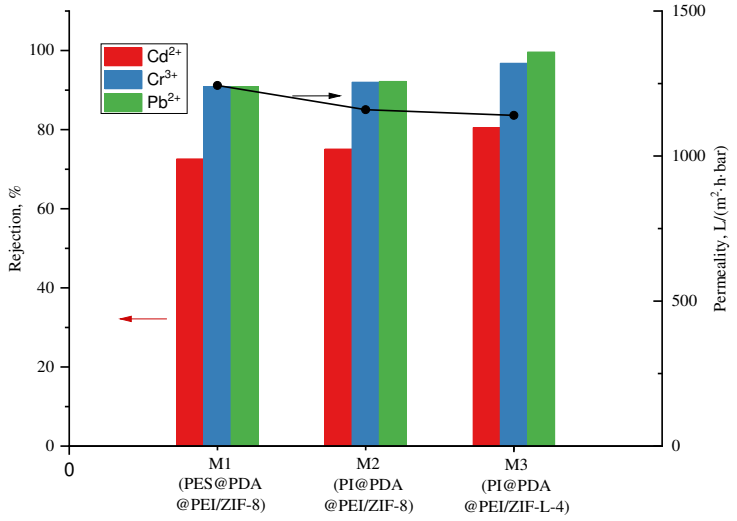

Figure 9. Water flux and heavy metal rejection of PI@PDA@PEI/ZIF-8 membrane and PI@PDA@PEI/ZIF-L-4 membrane.

3.4. Reusability of PI@PDA@PEI/ZIF-L-4 Composite Membranes

In applications the practical membrane should be reusable for cost purposes. A metal complexing agent, disodium ethylenediaminetetraacetic acid, is used for repeated tests of adsorption and desorption experiments in four cycles on the PI@PDA@PEI/ZIF-L-4 (5 wt.%) composite membrane, as shown in Figure 10.

As can be seen in the Figure 10, after two cycles of filtration, the membrane's removal rates of heavy metal ions were approximately decreased by 5%, 5%, and 20% for Cd^{2+}, Cr^{3+} and Pb^{2+}, respectively. After four cycles, the removal rates for Cd^{2+} decreased from 80.53% to 73.61%, for Cr^{3+} from 96.80% to 87.74%, and for Pb^{2+} from 96.63% to 85.43%, which means that the heavy metal removal rate was relatively stable. Thus, the PI@PDA@PEI/ZIF-L-4 composite membrane can perform four filtration cycles while maintaining a stable heavy metal removal rate. This suggests that the PI@PDA@PEI/ZIF-L-4 composite membrane is reusable with stable performances.

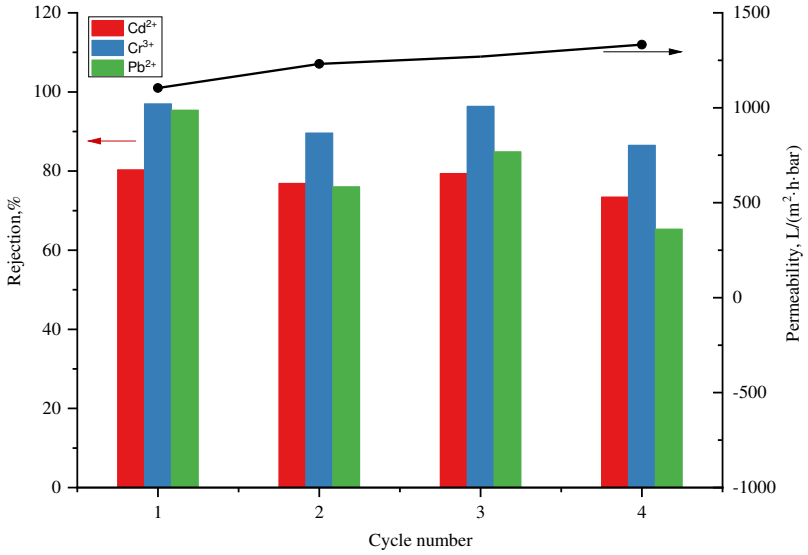

Figure 10. Heavy metal rejection and water flux of PI@PDA@PEI/ZIF-L-4 membrane during four filtration-washing cycles.

Preprints (www.preprints.org) | NOT PEER-REVIEWED | Posted: 11 October 2023 doi:10.20944/preprints202310.0653.v1

3.5. Exploration of Separation Mechanism of ZIF-L/PEI/PDA@PI Composite Membrane

The composite membranes prepared in this experiment are High Flux Separation Membranes permeating at low pressure. It is expected to adsorb heavy metal ions through the active sites in the membrane. EDX mapping was inspected on membranes as shown in Figure 11.

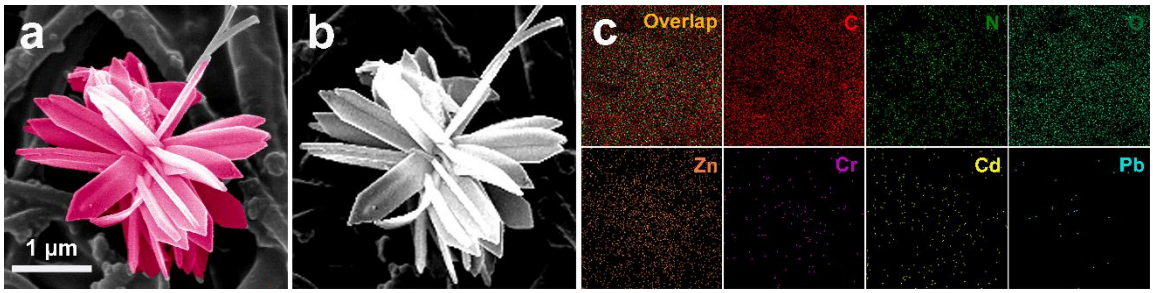

Figure 11. EDX mapping of the surface of the PI@PDA@PEI/ZIF-L-4 membrane after heavy metal adsorption.

As shown in Figure 12, Cd^{2+} and Cr^{3+} exist on the membrane surface, but Pb^{2+} was not detected. It can be confirmed that the adsorption of heavy metal ions does occur on the membrane surface. When the heavy metal ions are adsorbed on the membrane surface, the electrostatic repulsion between the incoming heavy metal ions in the solution and the adsorbed heavy metal ions will be conducive to the high exclusion of the incoming heavy metal ions. The content of lead is low, probably because Pb^{2+} has a smaller hydration energy, which is easier to enter the micropores of the adsorbent and also easier to enter the channels of ZIF-L-4. ZIF-L-4 adsorbs Pb^{2+} in pores through pores. Since ZIF-L-4 has a large size and many channels, the detection depth of EDX cannot reach the Pb^{2+} captured in the pores. The adsorption mechanism has to be verified by XPS.

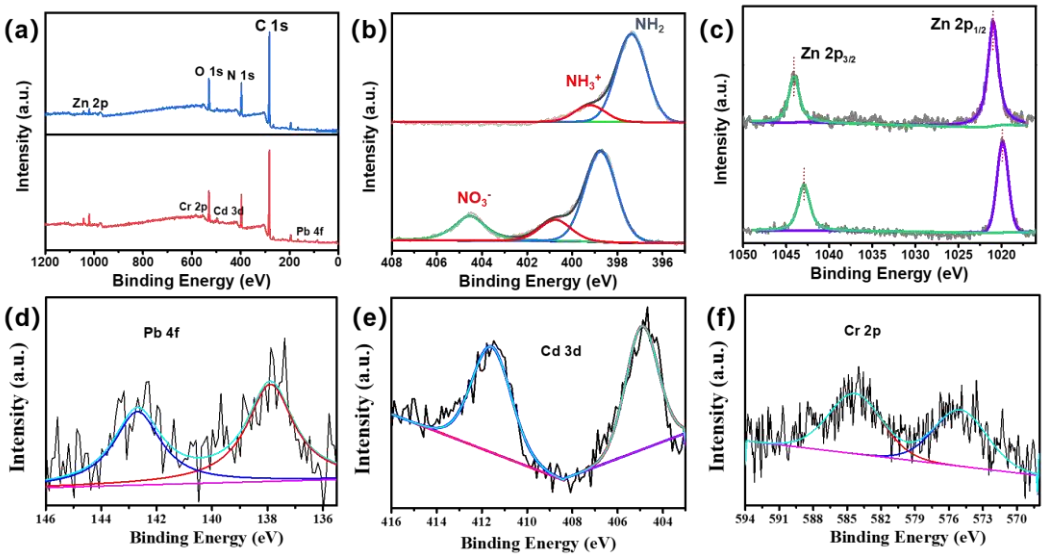

Figure 12. XPS spectra of (**a**) total (**b**) N 1s (**c**) Zn 2p (**d**) Pb 4f (**e**) Cd 3p (**f**) Cr 2p on the membrane surface before and after PI@PDA@PEI/ZIF-L-4 membrane adsorption.

As shown in Figure 12, peaks of Pb4f, Cd3d, and Cr2p appeared in the spectrum of XPS after adsorption, indicating that Cd^{2+}, Cr^{3+}, and Pb^{2+} were successfully adsorbed on the surface of the composite membrane. Before adsorption, the N 1s spectra were deconvoluted into two peaks at binding energies of 399.2 and 397.4 eV, corresponding to the neutral amine (–NH_2/–NH) and protonated amine (–NH_3^+ or -NH_2^+). With the filtration contacting with heavy metal ions in the feeding solution, the N 1s spectra of the composite film at binding energies of 404.5, 400.7, and

398.73eV were deconvoluted into three peaks. First, the new peak observed at 404.6ev corresponds to the nitrate (-NO_3-). The positive binding energy of the neutral and protonated amine is attributed to the binding of nitrogen atoms to heavy metal ions. Because the N atom shares lone pair electrons in the hybrid orbit coordinated between nitrogen and heavy metal ions, coordination bonds are formed, resulting in reduced electron cloud density, thus moving the binding energy to high energy [31]. Before adsorption, Zn2p peaked at 706.5 eV and 719.9 eV, demonstrating the presence of ZIF-L-4. After heavy metal adsorption, the Zn2p binding energy decreased and moved negatively, indicating that the chemical environment of Zn also changed. This is mainly due to the adsorption of heavy metal ions around Zn, changing the distribution state of its electron cloud, and Zn is also the active site of heavy metal adsorption.

4. Conclusions

PI@PDA@PEI/ZIF-L-4 and PI@PDA@PEI/ZIF-8 composite membranes were prepared, and the adsorption and separation performance and water flux of the two composite membranes for heavy metal ion solutions were tested and studied. The results show that, compared with the PI@PDA@PEI/ZIF-8 composite membrane, the PI@PDA@PEI/ZIF-L-4 composite membrane has higher adsorption and separation performance, and its removal rates of Cd^{2+}, Cr^{3+}, and Pb^{2+} increased by 7.0%, 6.6%, and 9.3%, respectively; the permeation flux reached 1,140.0 $L{\cdot}m^{-2}{\cdot}h^{-1}{\cdot}bar^{-1}$. The PI@PDA@PEI/ZIF-L-4 composite membrane's performances remained stable after four repeated uses.

References

1. Fu Fenglian, Wang Qi. Removal of heavy metal ions from wastewaters: a review[J]. Journal of environmental management, 2011, 92(3): 407-418.
2. Li Zhiming. A Brief Discussion on Spectral Detection Technology of Heavy Metals in Water[J]. Leather Manufacture and Environmental Technology,2022,3(23):17-18,31.
3. Zhou Ailing; Jia Aizhong; Zhao Xinqiang, etal. Wang Yanji. Research Progress on Selective Adsorption of Heavy Metal Ions in Sewage[J]. Materials Reports,2023,37(9):46-55.
4. Zheng Xikun, Lu Anhuai, Gao Xiang, et al. Contamination of heavy metals in soil present situation and method[J]. Soil and Environmental Sciences, 2002(01): 79-84.
5. Wang Shaozhen, Zang Biao, Chang Yueyue, et al. Synthesis and carbon dioxide capture properties of flower-shaped zeolitic imidazolate framework-L[J]. CrystEngComm, 2019, 21(43): 6536-6544.
6. Yan Liu, Rui Lv, Shiyong Sun, et al. High-performance cascade nanoreactor based on halloysite nanotubes-integrated enzyme-nanozyme microsystem[J]. Chinese Chemical Letters,2022,33(2):807-811.
7. Awadallah-F, Ahmed, Hillman, Febrian, Al-Muhtaseb, Shaheen A., et al. On the nanogate-opening pressures of copper-doped zeolitic imidazolate framework ZIF-8 for the adsorption of propane, propylene, isobutane, and n-butane[J]. Journal of Materials Science,2019,54(7):5513-5527.
8. Yizhak Marcus. Thermodynamics of solvation of ions. Part 5.—Gibbs free energy of hydration at 298.15 K[J]. Journal of the Chemical Society, Faraday Transactions, 1991, 87(18): 2995-2999.
9. Qi Yawei, Zhu Lifang, Shen Xin, et al. Polythyleneimine-modified original positive charged nanofiltration membrane: removal of heavy metal ions and dyes[J]. Separation and Purification Technology, 2019, 222: 117-124.
10. Peng Qiuming, Guo Jianxin, Zhang Qingrui, et al. Unique lead adsorption behavior of activated hydroxyl group in two-dimensional titanium carbide[J]. Journal of the American Chemical Society, 2014, 136(11): 4113-4116.
11. Zhou Long, Li Na, Jin Xiaoying, et al. A new nFe@ ZIF-8 for the removal of Pb (II) from wastewater by selective adsorption and reduction[J]. Journal of Colloid and Interface Science, 2020, 565: 167-176.
12. Al-Ghouti M A, Da'ana D A. Guidelines for the use and interpretation of adsorption isotherm models: A review[J]. Journal of hazardous materials, 2020, 393: 122383.
13. Foo K Y, Hameed B H. Insights into the modeling of adsorption isotherm systems[J]. Chemical engineering journal, 2010, 156(1): 2-10.
14. Fang Ying, Wen Jia, Zeng Guangming, et al. Effect of mineralizing agents on the adsorption performance of metal–organic framework MIL-100 (Fe) towards chromium (VI)[J]. Chemical Engineering Journal, 2018, 337: 532-540.
15. Li Bing, Zheng Jiaqi, Guo Jianzhong, et al. A novel route to synthesize MOFs-derived mesoporous dawsonite and application in elimination of Cu (II) from wastewater[J]. Chemical Engineering Journal, 2020, 383: 123174.

16. Changkun Liu, Renbi Bai, Quan San Ly. Selective removal of copper and lead ions by diethylenetriamine-functionalized adsorbent: Behaviors and mechanisms[J]. Water Research, 2008, 42(6-7): 1511-1522.
17. Zhang Yujie, Xie Zhiqiang, Wang Zhuqing, et al. Unveiling the adsorption mechanism of zeolitic imidazolate framework-8 with high efficiency for removal of copper ions from aqueous solutions[J]. Dalton Transactions, 2016, 45(32): 12653-12660.
18. Jimenez-Solomon M F, Gorgojo P, Munoz-Ibanez M, et al. Beneath the surface: Influence of supports on thin film composite membranes by interfacial polymerization for organic solvent nanofiltration[J]. Journal of membrane science, 2013, 448: 102-113.
19. Marchetti P, Jimenez Solomon M F, Szekely G, et al. Molecular separation with organic solvent nanofiltration: a critical review[J]. Chemical reviews, 2014, 114(21): 10735-10806.